Journal of Applied Polymer Science

Near-infrared-active and pH-responsive fluorescent polymer-integrated hybrid graphene oxide nanoparticles for the detection and treatment of cancer

Shazid Md. Sharker,[1] Eun Bi Kang,[2] Chun-Im Shin,[2] Sung Han Kim,[3] Gibaek Lee,[2] Sung Young Park[2,3]

[1]Department of Chemistry, Korea Advanced Institute of Science and Technology (KAIST), Daejeon 305-702, Republic of Korea
[2]Department of Chemical and Biological Engineering, Korea National University of Transportation, Chungju 380-702, Republic of Korea
[3]Department of IT Convergence, Korea National University of Transportation, Chungju 380-702, Republic of Korea
S. M. Sharker and E. B. Kang contributed equally to this article.
Correspondence to: S. Y. Park (E-mail: parkchem@ut.ac.kr)

ABSTRACT: Hybrid nanoparticles for theragnosis have great potentiality to bring desire functionalities in one integrated system. The development of bioimaging guided photothermal therapy (PTT) is pivotal in optimizing cytotoxic cancer therapy. We report near-infrared (NIR)-active and pH-responsive fluorescent, catechol-conjugated, reduced graphene oxide (rGO)-anchored hybrid nanoparticles that can sharply increase the photothermal heat in response to NIR exposure and exhibit pH-dependent fluorescence emission for the detection of tumor areas without causing cell toxicity. The optoelectronic absorption property of poly(3,4-ethylenedioxythiophene) [PEDOT]:dopamine-conjugated poly(4-styrenesulfonate-co-maleic acid) [D-PSM] and 3′,4′-dihydroxyacetophenone/boron-dipyrromethene [CCDP/BODIPY]-quaternized polyethylene glycol grafted poly(dimethylaminoethyl methacrylate) (C/B-PgP) present in this hybrid nanoparticles resulted in efficient photothermal conversion with pH-tunable fluorescence that exerted sufficient photothermal cytotoxicity to cancer cells. The *in vitro* cellular uptake was measured by confocal laser scanning microscopy, allowing the therapeutic efficiency and bioimaging effects to be explored. We expect that the broad optical absorption property of PEDOT:D-PSM with BODIPY-conjugated polymers on rGO sheets would get tremendous attraction in this enormous rising PTT with cancer detectable biomarker. © 2016 Wiley Periodicals, Inc. J. Appl. Polym. Sci. **2016**, *133*, 43791.

KEYWORDS: applications; biocompatibility; biomaterials; drug delivery systems; stimulisensitive polymers

Received 16 February 2016; accepted 18 April 2016
DOI: 10.1002/app.43791

INTRODUCTION

Fast recovery, fewer complications, and shorter hospitalization periods have made photothermal therapy (PTT) a preferred choice of medical treatment than the others methods, such as surgery, radiation therapy, and chemotherapy, which are responsible for severe side effects.[1] The so-called hyperthermia therapy, a form of PTT, uses near-infrared (NIR) light (690–900 nm) to target NIR-absorbing photothermal agents by converting external stimuli into heat, in turn killing the tumor cells through photo-thermolysis.[2] To develop NIR-active PTT agents, nanomaterials with high optical absorption properties such as gold nanostructures, carbon nanomaterials, magnetic nanoparticles, copper sulfide nanoparticles, and organic NIR dye-based materials have been widely explored by many research groups.[3] However, previous studies have mostly focused on non-biodegradable inorganic nano-metallic sources that are not biocompatible, and only limited studies have reported alternative sources.[4]

Hybrid nanomaterials are typically composed of both inorganic and organic components. They have recently been identified as promising platforms for theranostic applications. Hybrid designs not only take advantage of the beneficial features of both inorganic and organic components, but also provide the ability to systematically tune the desired properties through a combination of functional components.[5,6] Organic light-absorbing components are commonly studied in energy devices and OLED (organic light emitting diode) research.[7,8] However, they have been less extensively explored for photothermal

Additional Supporting Information may be found in the online version of this article.

applications, except in recent studies on polyaniline, poly-(3,4-ethylenedioxythiophene):poly(4-styrenesulfonate) (PEDOT:PSS), and polypyrrole.[9–12] Furthermore, a number of PTT agents have gained considerable attention because they incorporate diagnosis clue.[13] In this perspective, imaging-guided therapeutic systems promise more advantages than that with the single therapeutic or diagnosis agents. Recently, the chemical modification of graphene oxide has attracted interest in a wide range of applications because modified graphene-based materials have exhibited substantial thermal properties, mechanical properties, and colloidal stability.[14] Along with these interesting properties, the quenching capability of graphene oxide has demonstrated efficacy in the control of fluorescent materials. Graphene oxide surfaces have been suggested as an optimal quencher to regulate fluorescence tuning compared to the other carbon derivatives such as graphite, carbon nanotubes, and carbon nanofibers.[15]

In our work, we developed a new class of bioimaging hybrid PTT agents with a pH-responsive, nano-sized, and reduced form of graphene oxide (rGO) embedded in organic PEDOT:D-PSM [poly(3,4-ethylenedioxythiophene) with dopamine-conjugated poly(4-styrenesulfonate-co-maleic acid)] with polyethylene glycol grafted poly(dimethylaminoethyl methacrylate)[-PEG-*g*-PDMA]-quaternized BODIPY composite materials based on the catechol moiety (C/B-PgP). Catechol (CCDP) functionalized on both the PEDOT:D-PSM and C/B-PgP composite materials facilitated integrated anchoring on the rGO sheets [rGO/[PEDOT:D-PSM]:C/B-PgP]. A key advantage of this hybridization system is PEDOT:D-PSM acting as an optoelectro-active material for NIR light absorption, and the carbon-based rGO cooperatively absorbs light from the UV to NIR regions of the electromagnetic spectrum. Together, they are combined to enhance the photothermal conversion through non-radiative decay. In a parallel effort, BODIPY-conjugated PEG-g-PDMA, as a pH-responsive fluorescent component within this same hybrid system, acts as a stimulus-responsive cell imaging guided PTT agent.

EXPERIMENTAL

−3′,4′-dihydroxyacetophenone (CCDP), dopamine hydrochloride, ethanol, tetrahydrofuran, HCl, Trizma base (99%), Trizma HCl (99%), diethyl ether, hexane, and 3-(4,5-dimethylthiazol-2-yl)−2,5-diphenylterazolium bromide (MTT) were purchased from Sigma-Aldrich, Korea. Propidium iodide, calcein AM, and LysoTracker Blue DND-22 were purchased from Molecular Probe, Life Technologies (Invitrogen). Penicillin-streptomycin, fetal bovine serum, 0.25% (w/v) trypsin, 0.03% (w/v) ethylenediaminetetraacetic acid solution, and RPMI-1640 cells culture medium were purchased from Gibco BRL (Carlsbad, CA). CCDP- and BODIPY-quaternized[16,17] polyethylene glycol grafted poly(dimethylaminoethyl methacrylate) (PEG-*g*-PDMA) (C/B-PgP)[18] and dopamine-conjugated poly(sodium 4-styrenesulfonate-co-maleic acid) (D-PSM)[19] were synthesized as described in our previous reports.

UV-vis spectra were recorded using Optizen 2020UV, Mecasys Co. Atomic force microscopy (AFM) was performed in tapping mode on a MultiMode8 apparatus (Bruker) with a silicon probe. For AFM, samples were prepared on silicon wafers. An infrared camera was used (NEC Avio, Thermo Tracer TH9100). Particle size was measured using dynamic light scattering (DLS) (Zetasizer Nano, Malvern-Germany). X-ray photoelectron spectroscopy (XPS) was performed using an Omicrometer ESCA-LAB (Omicrometer, Taunusstein, Germany). Photoluminescence (PL) spectra were obtained from a L550B luminescence spectrometer from Perkin Elmer. Zeta potential data were obtained using a particle size analyzer (ELS-Z) from Otsuka Electronics Corporation. The NIR laser had a wavelength of 808 nm (PSU-III-LRD, CNI Optoelectronics Tech. Co. LTD, China). A Multimode microplate reader Filter MaxF3 (Molecular Devices, LLC.) was used for MTT assay.

Synthesis of Ionic Complex Poly(3,4-ethylenedioxythiophene) with Dopamine-Conjugated Poly(4-styrenesulfonate-co-maleic acid) [PEDOT:D-PSM]

PEDOT was conjugated with D-PSM by ionic complexation. First, 0.1 g of D-PSM and 1 g of PEDOT were added into 150 mL of 0.1 M HCl solution and the mixture was sonicated for 30 min. After magnetic stirring for 24 h at room temperature under nitrogen flow, the resulting ionic complex was dialyzed (molecular weight cut-off 1,000, Spectrum Laboratories Inc.), purified, and freeze-dried to obtain PEDOT:D-PSM with a yield of 80%.

Preparation of PEDOT:D-PSM And C/B-PgP-Anchored Reduced Graphene Oxide (rGO) via Catechol Chemistry rGO/[PEDOT:D-PSM]:C/B-PgP

To synthesize a combined optoelectric conductive PEDOT:D-PSM and fluorescent C/B-PgP-anchored reduced graphene oxide (rGO) hybrid material, PEDOT:D-PSM (70 mg) and C/B-PgP (150 mg) were mixed with rGO (1 mg) in TBS buffer at pH 8.5. The reaction was continued for 12 h at room temperature. The mixture was finally centrifuged (4000 rpm, 4 min) and freeze-dried to obtain rGO/[PEDOT:D-PSM]:PgP (yield = 80%).

MTT Assay

Cytotoxicity was measured using an [3-(4,5-dimethylthiazol-2-yl)-2,5-diphenyltetrazolium bromide] MTT assay method. Here, 200 μL of KB cells (human *epidermoid* carcinoma cells) and MDAMB-231 cells (human *breast cancer* cells), at a density of 2×10^5 cells/mL, were placed in each well of a 96-well plate. Afterwards, the cells were incubated for 24 h at 37 °C in a humidified 5% CO_2 atmosphere. To determine the cell viability, a stock solution of rGO/[PEDOT:D-PSM]:C/B-PgP was dissolved in RPMI medium at a concentration of 1 mg/mL and the stock solution was diluted to 0.01 mg/mL. The medium was removed and the cells were treated with different concentrations of rGO/[PEDOT:D-PSM]:C/B-PgP. The cells were then incubated as previously described for another 24 h. The medium containing rGO/[PEDOT:D-PSM]:C/B-PgP was then replaced with 180 μL of fresh medium and 20 μL of stock solution containing 15 mg of MTT in 3 mL of PBS and incubated for another 4 h. Finally, the medium was removed and 200 μL of MTT solubilizing agent was added to the cells with 15 min of accurate shaking. Absorbance was measured at 570 nm using a microplate reader. The relative cell viability was measured by comparing the control 96-well plate containing only cells.

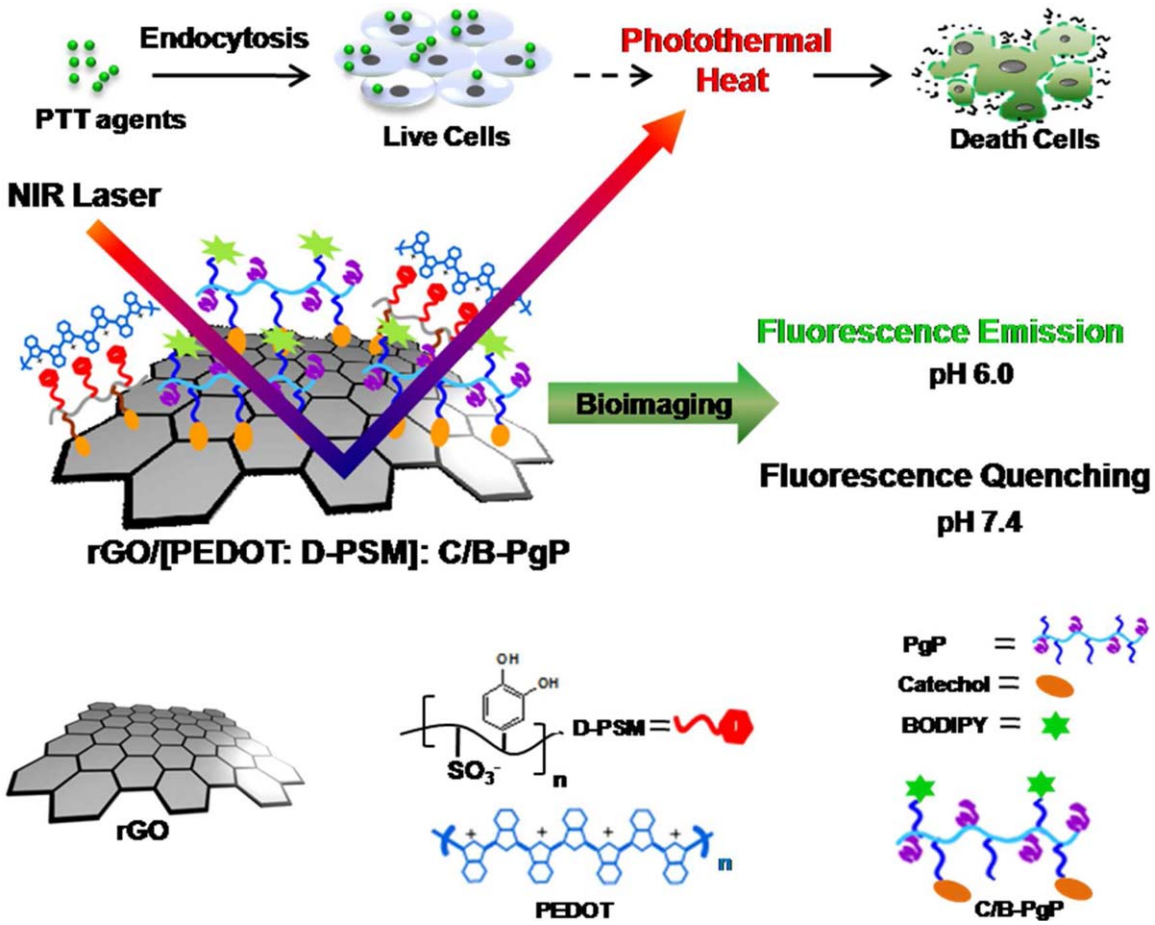

Figure 1. Schematic illustration of the preparation of hybrid photothermal agents based on organic PEDOT: D-PSM and fluorescent polymeric composite C/B-PgP anchored rGO/[PEDOT: D-PSM]: C/B-PgP and their pH responsive bioimaging index, and NIR light responsive photothermal activation to ablate tumor by using NIR laser irradiation. [Color figure can be viewed in the online issue, which is available at wileyonlinelibrary.com.]

In Vitro Photothermal Cytotoxic Assay

The photothermal cytotoxicity of rGO/[PEDOT:D-PSM]:C/B-PgP was evaluated in MDAMB cells and KB cells. First, 200 μL of KB cells were placed in each well of a 96-well plate at a density of 2×10^5 cells/mL. The cells were then incubated for 24 h at 37 °C in a humidified 5% CO_2 atmosphere. To assess the *in vitro* photothermal effect of rGO/[PEDOT:D-PSM]:C/B-PgP, the cell culture growth medium was replaced with medium containing rGO/[PEDOT:D-PSM]:C/B-PgP at concentrations of 1 mg/mL to 0.01 mg/mL. After replacing the medium, the cells were incubated in 96-well plates at 37 °C for 30 min. They were then irradiated with an 808-nm laser at a power density of 2 W/cm^2 for 5 min and incubated for another 24 h. The viability and proliferation of the MDAMB cells and KB cells were evaluated by an MTT assay.

Calcein AM and Propidium Iodide Cell Staining Assay

Cell viability of photothermal cytotoxicity was evaluated through the calcein AM (calcein acetoxymethyl ester) and propidium iodide (PI) co-staining methods described in literature.[20] To assess the photothermal effect, the KB cells were incubated in cell culture medium with rGO/[PEDOT:D-PSM]:C/B-PgP at a concentration of 0.2 mg/mL for 30 min in 8-well plates at 37 °C. At the end of the incubation, the cells were irradiated with an 808-nm laser at a power density of 2 W/cm^2 for 5 min. The cells were then stained with both calcein AM and PI. Finally, an LSM510 confocal laser scanning microscope (Carl Zeiss, Germany) was used to take images of stained (live/dead) cells at 10× magnification.

Confocal Imaging

The cellular uptake of photothermal rGO/[PEDOT:D-PSM]:C/B-PgP was analyzed by confocal imaging. KB cells were plated over a cover slide on an 8-well plate at a density of 2×10^5 cells/mL per well and incubated for 24 h at 37 °C in a humidified 5% CO_2 atmosphere. Afterwards, the cells were treated with rGO/[PEDOT:D-PSM]:C/B-PgP at 0.01 mg/mL for 30 min, in fresh culture medium at pH 5.0, 6.0, 6.8, and 7.4. HCl (0.1 *N*) and NaOH (0.1 *N*) were used to adjust the pH of the culture medium. The cells were then washed with PBS several times to remove the unbound rGO/[PEDOT:D-PSM]:C/B-PgP. The negative control cells imaging were studied by using as-prepared hybrid nanoparticles without taking BODIPY parts. Finally, the cells were examined at 20× magnification using an LSM510 confocal laser scanning microscope (Carl Zeiss, Germany).

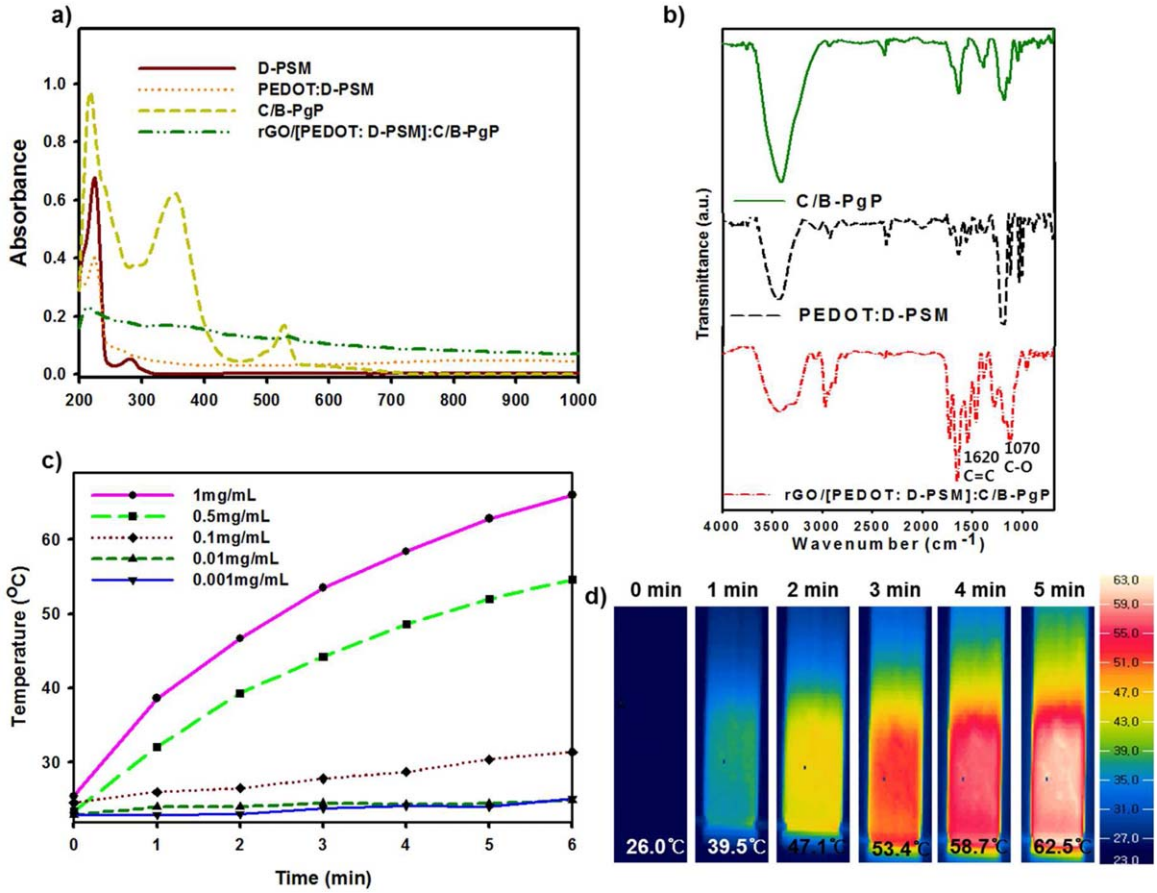

Figure 2. The evaluation of optical absorption and photothermal conversion. (a) The UV-vis absorption of D-PSM, PEDOT:D-PSM:C/B-PgP and rGO/[PEDOT:D-PSM]:C/B-PgP hybrid material. (b) The FT-IR peaks of PEDOT:D-PSM:C/B-PgP and rGO/[PEDOT:D-PSM]:C/B-PgP hybrid material. (c) The concentration dependent photothermal conversion capability of rGO/[PEDOT:D-PSM]:C/B-PgP hybrid material as a function of NIR (808 nm laser) irradiation time. The solvent in this study was water (DW). (d) The NIR irradiated thermographic image of a solution of rGO/[PEDOT: D-PSM]:C/B-PgP (1 mg/mL) from 1 min to 5 min. [Color figure can be viewed in the online issue, which is available at wileyonlinelibrary.com.]

RESULTS AND DISCUSSION

Development for the formation of Photothermal Hybrid Nanostructure

PTT employs NIR pinpoint-responsive thermo-active agents to enable tumor destruction by a laser-guided light source.[21] Well-designed functional materials with bioimaging and photothermal ablation abilities can maintain such payloads by distinguishing malignant areas to avoid unwanted damages in normal human tissues.[22] To design such functional materials, hybrid constructions represent an emerging route towards acquiring desired poly-functional materials.pH-responsive bioimaging is useful at the interface between normal tissues and abnormal tumor mass. We attached the pH-sensitive fluorescent polymer C/B-PgP, whose emission increases with decreasing pH, in rGO sheets.[23,24] The final developed rGO/[PEDOT:D-PSM]:C/B-PgP hybrid particle was therefore expected to show excellent pH-sensitive bright fluorescence and efficient photothermal conversion because it took advantage of the conductivity broad band optical absorption properties of the PEDOT:D-PSM moiety (Figure 1).[25] More importantly, because we chose a conductive polymer (PEDOT:D-PSM), it can also assist in the photo-activation of the supporting graphene sheet base, which has a broad UV-vis-NIR absorption nature. Therefore, we can conveniently select any suitable NIR wavelength (600–900 nm), which will be flexible for clinical applications.[26]

The Spectroscopic Properties and Photothermal Heat Generation

The UV-vis absorption spectrum of the D-PSM (dopamine-conjugated poly(4-styrenesulfonate-co-maleic acid)), PEDOT:D-PSM, C/B-PgP, and rGO/[PEDOT:D-PSM]:C/B-PgP hybrid material is shown in Figure 2(a). D-PSM shows an absorption peak at around 280 nm, which is indicative of dopamine (D), whereas complexation of PEDOT with PSM exhibited significant absorption into the NIR region because of its low band gap (optical band gap).[27,28] The BODIPY absorption peak observed in the C/B-PgP fluorescent polymeric composite and rGO sheet exhibited an increase at around 550 nm into the NIR region.[20,26] This is due to the electric conductivity for the charge transfer of PEDOT on the rGO hybrid sheets as a result of increased electron delivery efficiency.[29,30] As a result of the optical absorption property in the NIR region, rGO/[PEDOT:D-PSM]:C/B-PgP can be considered as a well-suited photothermal agent for PTT. Figure 2(b) shows the KBr infrared (IR) absorption spectra of as-prepared rGO/[PEDOT:D-PSM]:C/B-PgP. The

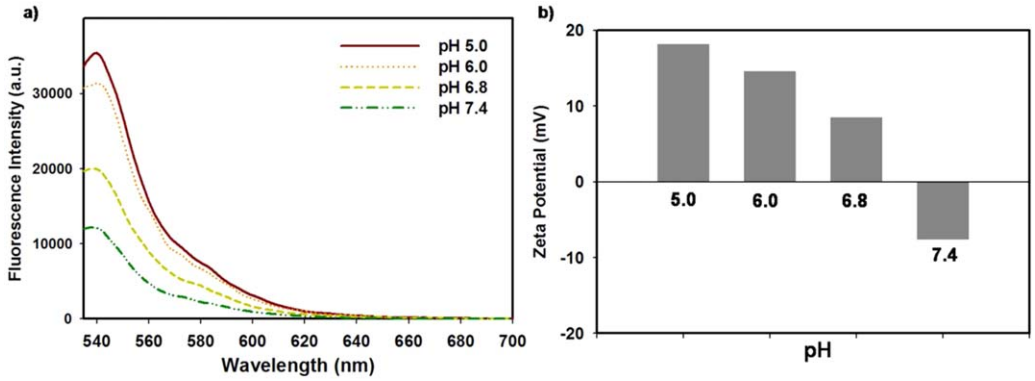

Figure 3. The characterization of fluorescence emission intensity and surface charge. (a) The pH responsive fluorescence emission curve in 526 nm excitation wavelength of rGO/[PEDOT: D-PSM]: C/B-PgP (0.1 mg/mL). (b) Changes in zeta potential (mV) for rGO/[PEDOT: D-PSM]: C/B-PgP hybrid nanoparticles (0.01 mg/mL) at different pH values in PBS. [Color figure can be viewed in the online issue, which is available at wileyonlinelibrary.com.]

intensity of the band at 1469 cm^{-1} is attributed to the bending of the C—H bond in —CH(CH_3)$_2$. The peak at 1549 cm^{-1} represents the tertiary amine of the DMA unit,[31] and the peaks at 3450 and 2919 cm^{-1} are characteristic indicators of the BODIPY moiety.[32] The band at 1521 cm^{-1} is ascribed to the stretching of C=C and C-C in the thiophene ring. Moreover, the peak at 1342 cm^{-1} may be due to the C=C stretching vibration of the thiophene unit in PEDOT.[33] After functional integration with PEDOT:D-PSM and C/B-PgP, rGO composites showed oxygen functional groups at around 3400 cm^{-1}, C=C groups around 1620 cm^{-1} and epoxy groups 1070 cm^{-1}, which became very weak compared to previous PEDOT:D-PSM and C/B-PgP components, indicating successful decoration on rGO sheets.[34,35] We then studied the photothermal conversion ability of rGO/[PEDOT:D-PSM]:C/B-PgP. This NIR-irradiated hybrid material showed rapidly rising photothermal heat as a function of irradiation time, and depending on the concentration (0.1 mg/mL to 1 mg/mL), the heat elevation curve sharply increased from 32 °C to 64 °C in 5 min [Figure 2(c,d)]. At the same time without hybridization, the rGO, PEDOT, PEDOT:D-PSM and C/B-PgP shows relatively less photothermal effects compare to hybrid nanoparticles rGO/[PEDOT:D-PSM]: C/B-PgP (Supporting Information Figure S1). Typically, PTT kills cancer cells by maintaining the temperature at 42 °C for 12–60 min, and this duration can be reduced to 4–6 min at 50 °C. Furthermore, the *in vivo* temperature of the human body is

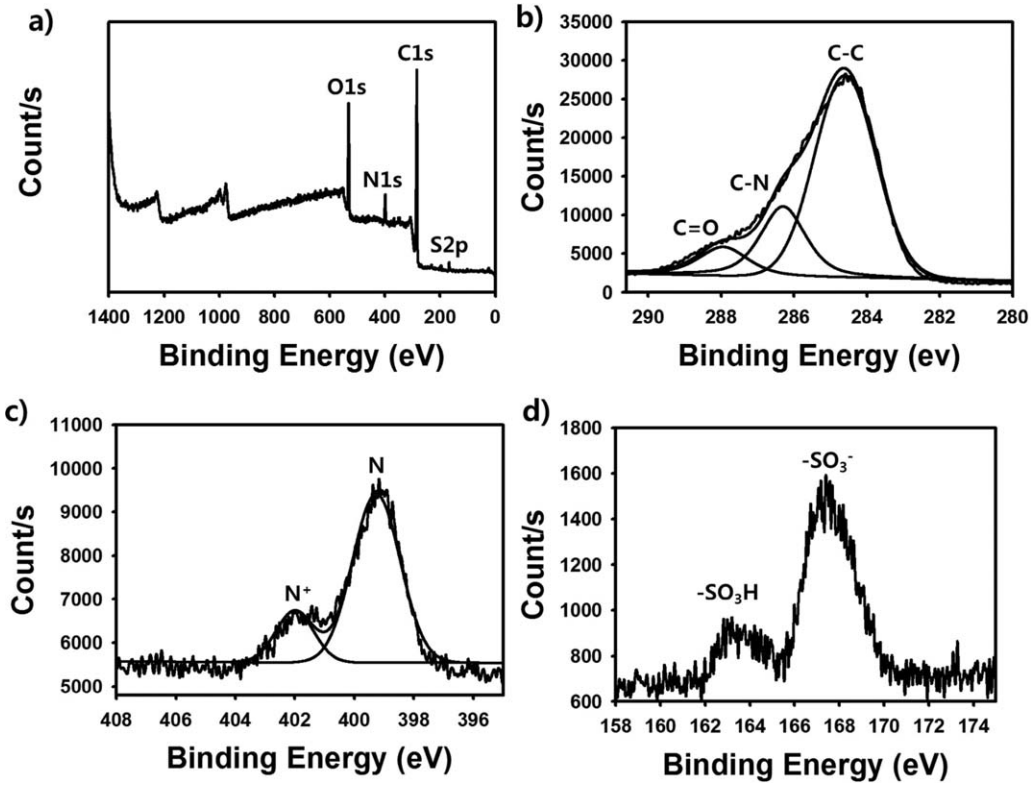

Figure 4. XPS measurements in (a) survey and narrow scan of (b) C1s, (c) N1s and (d) S2p of rGO/[PEDOT:D-PSM]:C/B PgP hybrid material.

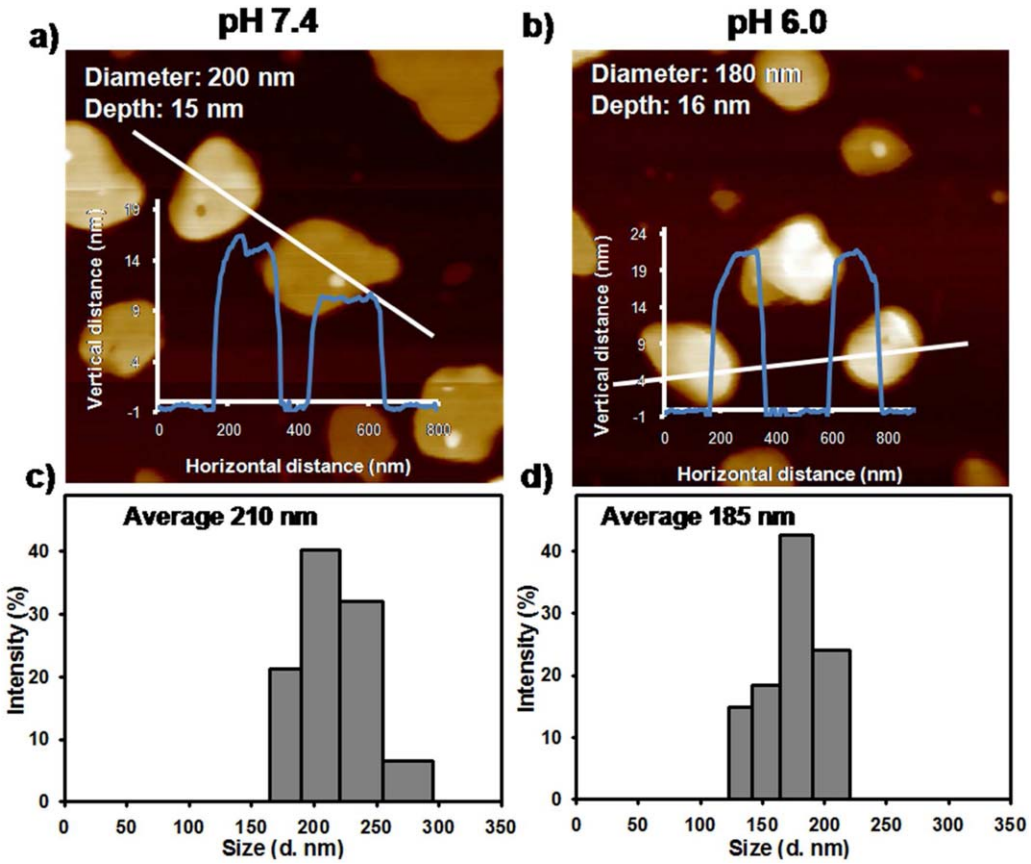

Figure 5. Atomic force microscope (AFM) images and height profile of a droplet of rGO/[PEDOT:D-PSM]:C/B-PgP hybrid nanoparticles at (a) pH 7.4 and (b) pH 6.0 in PBS. DLS measurements of nanocomposite at (c) pH 7.4 and (d) pH 6.0. [Color figure can be viewed in the online issue, which is available at wileyonlinelibrary.com.]

36 °C, which can be easily exceeded to reach over 50 °C within a short duration to efficiently kill cancer cells.[2]

Fluorescence Emission and Colloidal Stability Measurements

The detection of susceptible tumor areas is similarly important in anti-cancer therapy. The presence of C/B-PgP in this hybrid particle could be utilized for such detection.[24] In Figure 3, the fluorescence emission intensity of rGO/[PEDOT:D-PSM]:C/B-PgP increased with decreasing pH [Figure 3(a)] in the medium. The pH-responsive fluctuations in fluorescence are due to the hydrophilic DMA units at lower pH, which generate a gap between the rGO sheets and the polymer backbone that resulted in the bright green emission of BODIPY. Moreover, decreasing pH induced protonation that increased hydrophilicity in the polymeric backbone, which also resulted in bright emission from BODIPY.[24] Response to stimulus can be a promising regulator to detect cancer cells and to differentiate the tumor area.

In colloidal stability evaluation, the zeta potential (mV) was changed from positive (+19) to negative (−9) surface charge as the solution pH was increased from 5.0 to 7.4 [Figure 3(b)]. This is because under acidic condition, the cationic form of the composite material was protonated and solubilized, resulting in the exposure of the composite. As a result, PEDOT:D-PSM shows positive potentiality in response to increasing cationic form. However, in basic medium, the anionic form of the composite material was de-protonated and the composite was internalized on the rGO sheets, resulting in neutralized surface potentiality, which then turned into characteristic own negative potentiality.[36] Furthermore the stability and size distribution in cells culture medium and physiologic buffer solution (pH 7.4) was evaluated between 1 and 7 days, showing well dispersed and suspended rGO/[PEDOT:D-PSM]:C/B-PgP hybrid nanoparticles with time, suggesting uniform dispersity (Supporting Information Figure S2).

Characterization of Materials Composites

The composition of PEDOT:D-PSM-based rGO materials was characterized using XPS. The XPS survey of rGO/[PEDOT:D-PSM]:C/B-PgP shows the main peaks of C1s, N1s, and S2p centered at 285, 401, and 168 eV, respectively (Figure 4). The C1s core-line spectrum of the hybrid composite can be curve-fitted by three peak components with binding energies of around 284.5, 286.5, and 288 eV attributed to the C—C, C—N, and C═O species, respectively [Figure 4(b)].[24] The nitrogen core level spectrum revealed two components at 399 and 402 eV that are characteristic of the neutral amine (N^0) and cationic amine (N^+) form, respectively, demonstrating quaternization of PEG-*g*-PDMA [Figure 4(c)].[16] At the same time, an S2p peak appeared at 168 eV, indicating the presence of sulfonated groups. A peak near 167.2 eV was attributed to sulfur in the —SO_3H group [Figure 4(d)].[27]

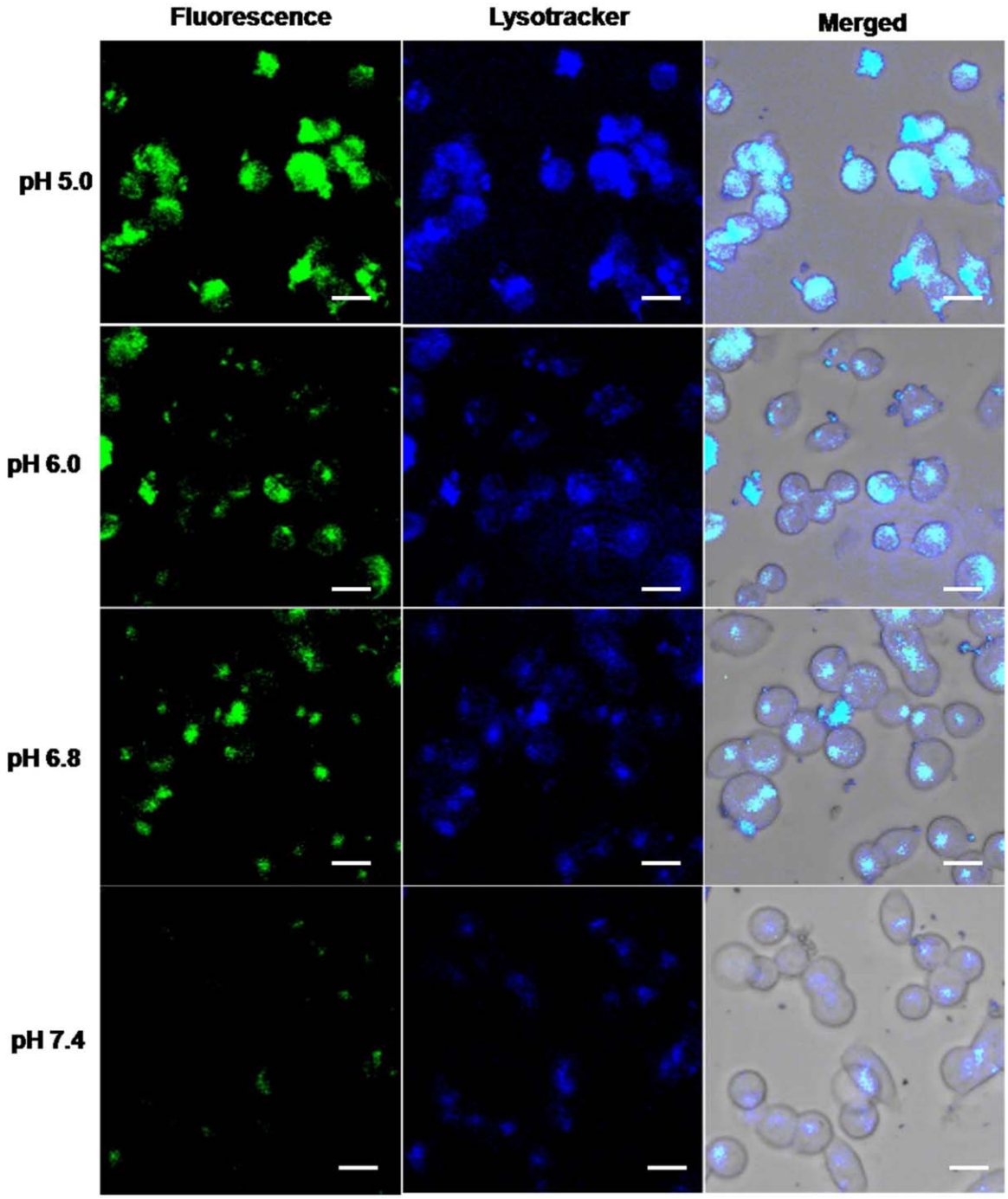

Figure 6. Confocal microscope co-stained images of KB cells under different pH (from 5.0 to 7.4) by using rGO/[PEDOT:D-PSM]:C/B-PgP hybrid nanoparticles (0.01 mg/mL) and Lysotracker blue. Scale bars: 20 μm and nanoparticles concentration: 0.01 mg/mL. [Color figure can be viewed in the online issue, which is available at wileyonlinelibrary.com.]

Particle Size and Size Distribution

The advantage of nanostructures in therapeutic systems is that their small size overcomes biological barriers and allows cellular uptake to occur.[37] The size of rGO/[PEDOT:D-PSM]:C/B-PgP hybrid nanoparticles was studied using AFM on an aqueous drop on silicon wafer, where the nanoparticles exhibited a diameter of ~200 nm to ~180 nm and a height profile of 15–16 nm, at pH 7.4 and 6.0, respectively [Figure 5(a,b)]. In addition, the morphology of the particles was almost spherical. The increase in thickness of approximately 10 nm suggested the hybridized composite materials on graphene oxide sheets. This hybridized might be due to the robust adhesion of marine mussels adhesive interactions between catechol and graphene oxide.[14] At the same time, the DLS measurements of the size of the hybrid nanoparticles dissolved in aqueous medium was comparable to the size distribution from the AFM

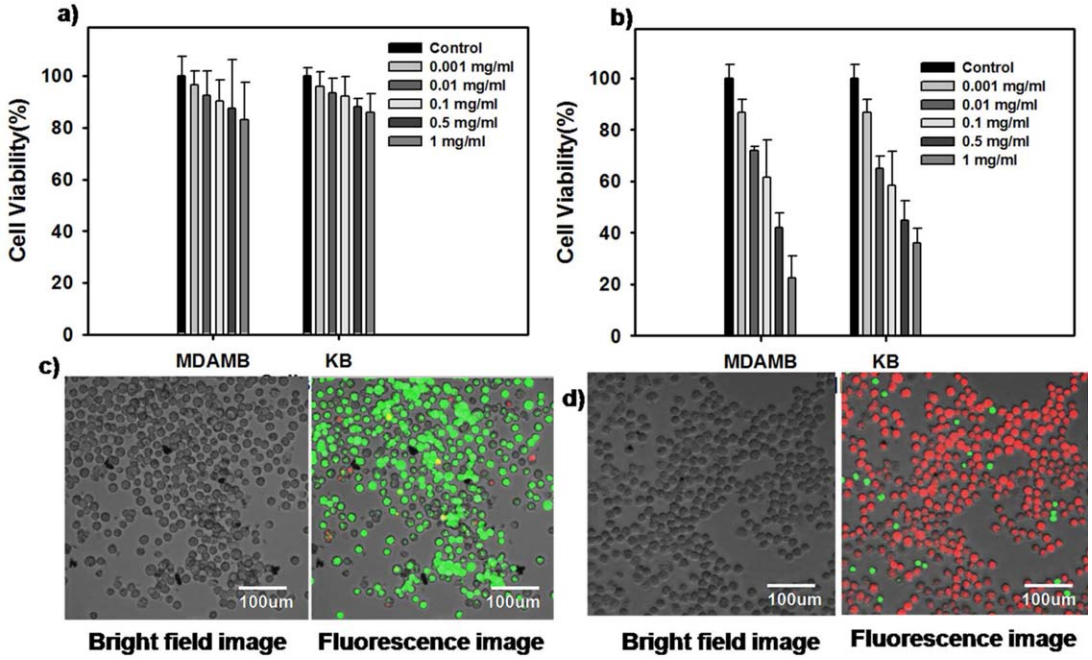

Figure 7. (a) The MTT assay for concentration dependent *in vitro* biocompatibility study of rGO/[PEDOT:D-PSM]:C/B PgP hybrid nanoparticles treated MDAMB and KB cells. (b) The NIR irradiated *in vitro* photothermal cytotoxicity of rGO/[PEDOT:D-PSM]:C/B-PgP hybrid nanoparticles in different concentration (1.0 mg/mL to 0.001 mg/mL). The calcein AM and propedium iodide co-stained live/dead cells fluorescence imaging of 0.2 mg/mL of rGO/[PEDOT:D-PSM]:C/B-PgP hybrid nanoparticles treated KB cells (c) without using NIR irradiation and (d) with using NIR irradiation. All the scale bars were 50 μm and NIR irradiation was 5 min, 808 nm laser intensity and 2 W/cm^2 power densities. [Color figure can be viewed in the online issue, which is available at wileyonlinelibrary.com.]

measurements [Figure 5(c,d)]. The magnitude of particle size is well described for efficient colloidal dispensability and passive diffusion for cellular uptake and endocytosis.

pH Responsive *In Vitro* Bioimaging

The advantage of stimulus-response fluorescent nanoparticles is that they can act as fluorescent bioimaging probes in microscopic techniques through tuning the stimulus signal.[38] In biological systems, the extracellular tumor pH is mildly acidic because of improper lymphatic drainage and metabolic acidosis. To track the tumor site, pH fluctuations are considered as a universal diagnostic route. Moreover, pH-sensitive delivery systems can be efficiently released from endosomal membrane after cellular uptake[39] In Figure 6, the KB cells incubated with rGO/[PEDOT:D-PSM]:C/B-PgP hybrid nanoparticles show increased bright fluorescent signals with decreasing pH (cell culture medium), indicating cellular uptake. Additionally, the Lysotracker (blue) co-stained cell image also shows overlaid co-localized lysosomes, which reasonably confirmed the localization of hybrid nanoparticles inside these cells. However, in absence of BODIPY moieties in the hybrid nanoparticles shows only stained lysosomes without noticeable fluorescent signals (Supporting Information Figure S3). The efficient cellular uptake indicates the potentiality of tumor cell detection and intracellular delivery.[40]

In Vitro Biocompatibility and Photothermal Activity

Biocompatibility and therapeutic efficiency are two prime criteria in the development of therapeutic ingredients.[41] The cell viability study from the MTT assay showed that the rGO/[PEDOT:D-PSM]:C/B-PgP hybrid nanoparticles exhibited concentration-independent biocompatibility. Even at a higher concentration (1 mg/mL), cell viability remained at approximately 93% in both MDAMB and KB cells [Figure 7(a)]. However, the cell viability changed drastically after exposure to NIR light. Cancerous MDAMB and KB cells treated with NIR-irradiated rGO/[PEDOT:D-PSM]:C/B-PgP hybrid nanoparticles clearly showed decreased cell viability as the concentration of hybrid nanoparticles increased, and less than 24% of the cells remained alive at a concentration of 1 mg/mL [Figure 7(b)]. This might be due to the high thermal conductivity of PEDOT:D-PSM on rGO sheets, which efficiently released thermal heat from the site of origin to the surrounding cytoplasm area.[42] The calcein AM and PI co-stained cells demonstrated a clear demarcation between live (green) and dead cells (red) [Figure 7(c)], without NIR irradiation and [Figure 7(d)] with NIR irradiation.[22] In the absence of NIR, the cell viability remained satisfactory, while the application of NIR light effectively killed the cancer cells, demonstrating photothermal cytotoxicity from photothermal heat. Indeed, PEDOT:PSM has been widely explored in optoelectronic devices including light-emitting diodes and photovoltaic cells because of its high conductivity, mechanical flexibility, and thermal stability. However, the applicable property of widely tunable spectra, from the visible to NIR region, is relatively less extensively explored, except in recent papers demonstrating the possibility of using 3,4-propylenedioxyselenophene (ProDOS) as a structural analog of

PEDOT for photothermal effects.[7,26,30] Thus, we expect that the photothermal applications of PEDOT:PSM and the pH-responsive bioimaging role of PgP on an integrated hybrid rGO structure will point to the direction of the development of various multifunctional PTT agents.[6,43]

Hybridized composite are therefore appears as a promising theragnosis platform for rationalizing cytotoxic cancer therapy and reducing adverse effects in patients care through the recombination of different functional clue, including bioimaging and controllable or stimuli-responsive drug delivery.[6] However, most of reviews have emphasized on carbon nanotube, silica and metal-organic based nanomaterials composed of organic and inorganic components.[4,6] In this study the tested optoelectronic absorption property of PEDOT:D-PSM on rGO nanoparticles resulted in efficient photothermal conversion with pH-tunable fluorescence against cancer cells. Though mussel adhesive dopamine mimic catechols have a strong anchoring affinity on the solid surface, the hybridization interactions between catechol and solid graphene oxide retained sufficient structural durability, particularly for critical biomedical application. The usefulness against cancer cells may have due to on demand therapeutic translation of functional clue in rGO nanoparticles.[44]

Virtually in all cases, the functional active agent in rGO base nanoparticles was associated with substantial biological activity resulting on-demand theragnosis performance. These findings extend those of recent reports, confirming that anchoring composite on the rGO sheets tending to stabilize, and activate more effective ways than when those composites are treating isolate form such as self assemble or blended form.[15,22,24,45] Taking advantage of catechol chemistry, the improvements noted in our study were independent to the type of active ingredients or functional moiety. This study therefore indicates that the benefits gained from rGO-catechol intervention may address hybridization needs across a wide range of nanoparticles.[46] Most notably, this is the first study to our knowledge to investigate the effectiveness of optoelectronic absorption property of PEDOT on rGO sheets whose photothermal conversion is itself thought to be bio-activation. Our results provide compelling evidence for hybrid nanoparticles development with such rGO and suggest that this approach appears to be effective in multifunctional nanoparticles that may overcome challenge of the detection and treatment of cancer.

CONCLUSIONS

In summary, we have introduced [PEDOT:D-PSM]:C/B-PgP-anchored rGO hybrid photothermal agents for cancer cell ablation. The in-cooperation of pH-responsive fluorescent polymeric composites on this hybrid structure cooperatively performed tumor area optimization via the bioimaging of cancer cells. XPS measurements revealed the hybridized structure while AFM, DLS, and zeta potential results clearly described colloidal stability. These nanosize hybrid particles also demonstrated pH-dependent fluorescence emission, and efficient *in vitro* internalization was confirmed by confocal laser scanning microscopy. After NIR irradiation, the cellular uptake from this hybrid nanoparticle resulted in the photothermal destruction of treated cells. Together with guided cell imaging, the photothermal hybrid agent on the integrated rGO system would add a new specificity to adopt optoelectric property in exploring alternative photothermal agents.

ACKNOWLEDGMENTS

This work was supported by the Grant No. 10048377, 10062079 and R0005237 from the Ministry of Trade, Industry & Energy (MOTIE), and Fusion Research R&D Program from the Korea Research Council for Industrial Science & Technology (No. G02054), Basic Science Research Program through the National Research Foundation of Korea (NRF) funded by the Ministry of Education (No. 2014055946).

REFERENCES

1. Hu, K. W.; Huang, C. C.; Hwu, J. R.; Su, W. C.; Shieh, D. B.; Yeh, C. S. *Chem. Eur. J.* **2008**, *14*, 2956.
2. Mackey, M. A.; Ali, M. R. K.; Austin, L. A.; Near, R. D.; El-Sayed, M. A. *J. Phys. Chem. B* **2014**, *118*, 1319.
3. Lim, D. K.; Barhoumi, A.; Wylie, R. G.; Reznor, G.; Langer, R. S.; Kohane, D. S. *Nano Lett.* **2013**, *13*, 4075.
4. Sun, T.; Zhang, Y. S.; Pang, B.; Hyun, D. C.; Yang, M.; Xia, Y. *Angew. Chem. Int. Ed.* **2014**, *53*, 12320.
5. Mehdi, A.; Reye, C.; Corriu, R. *Chem. Soc. Rev.* **2011**, *40*, 563.
6. Taylor-Pashow, K. M. L.; Rocca, J. D.; Huxford, R. C.; Lin, W. *Chem. Commun.* **2010**, *46*, 5832.
7. Groenendaal, L.; Jonas, F.; Freitag, D.; Pielartzik, H.; Reynolds, J. R. *Adv. Mater.* **2000**, *12*, 481.
8. Yook, K. S.; Lee, J. Y. *J. Ind. Eng. Chem.* **2015**, *23*, 179.
9. Yang, J.; Choi, J.; Bang, D.; Kim, E.; Lim, E. K.; Park, H.; Suh, J. S.; Lee, K.; Yoo, K. H.; Kim, E. K.; Huh, Y. M.; Haam, S. *Angew. Chem. Int. Ed.* **2011**, *50*, 441.
10. Li, L.; Liu, Y.; Hao, P.; Wang, Z.; Fu, L.; Ma, Z.; Zhou, J. *Biomaterials* **2015**, *41*, 132.
11. Yang, K.; Xu, H.; Cheng, L.; Sun, C.; Wang, J.; Liu, Z. *Adv. Mater.* **2012**, *24*, 5586.
12. Chen, M.; Fang, X.; Tang, S.; Zheng, N. *Chem. Commun.* **2012**, *48*, 8934.
13. Yao, J.; Yang, M.; Duan, Y. *Chem. Rev.* **2014**, *114*, 6130.
14. Kang, S. M.; Park, S.; Kim, D.; Park, S. Y.; Ruoff, R. S.; ; Lee, H. *Adv. Funct. Mater.* **2011**, *21*, 108.
15. Morales-Narváez, E.; Merkoçi, A. *Adv. Mater.* **2012**, *24*, 3298.
16. Mosaiab, T.; In, I.; Park, S. Y. *Macromol. Rapid Commun.* **2013**, *34*, 1408.
17. Garcıa-Moreno, I.; Costela, A.; Campo, L.; Sastre, R.; Amat-Guerri, F.; Liras, M.; Arbeloa, F. L.; Banuelos Prieto, J.; Arbeloa, I. L. *J. Phys. Chem. A* **2004**, *108*, 3315.
18. Nam, J. A.; Nahain, A. A.; Kim, S. M.; In, I.; Park, S. Y. *Acta Biomater.* **2013**, *9*, 7996.
19. Kim, S. M.; Lee, J.; In, I.; Park, S. Y. *Chem. Lett.* **2014**, *43*, 1453.

20. Sharker, S. M.; Kim, S. M.; Lee, J. E.; Choi, K. H.; Shin, G.; Lee, S.; Lee, K. D.; Jeong, J. H.; Lee, H.; Park, S. Y. *J. Control. Release* **2015**, *217*, 211.
21. Sharker, S. M.; Kim, S. M.; Kim, S. H.; In, I.; Lee, H.; Park, S. Y. *J. Mater. Chem. B* **2015**, *3*, 5833.
22. Sharker, S. M.; Lee, J. E.; Kim, S. H.; Jeong, J. H.; In, I.; Lee, H.; Park, S. Y. *Biomaterials* **2015**, *61*, 229.
23. Yu, J.; Chu, X.; Hou, Y. *Chem. Commun.* **2014**, *50*, 11614.
24. Sharker, S. M.; Jeong, C. J.; Kim, S. M.; Lee, J. E.; Jeong, J. H.; In, I.; Lee, H.; Park, S. Y. *Chem. Asian J.* **2014**, *9*, 2921.
25. Rousseau, T.; Cravino, A.; Bura, T.; Ulrich, G.; Ziessel, R.; Roncali, J. *Chem. Commun.* **2009**, 1673.
26. Kim, B.; Kim, J.; Kim, E. *Macromolecules* **2011**, *44*, 8791.
27. Hwang, J.; Amy, F.; Kahn, A. *Org. Electron.* **2006**, *7*, 387.
28. Lee, M. S.; Lee, J. E.; Byun, E.; Kim, N. W.; Lee, K.; Lee, H.; Sim, S. J.; Lee, D. S.; Jeong, J. H. *J. Control. Release* **2014**, *192*, 122.
29. Xia, Y.; Ouyang, J. *ACS Appl. Mater. Interfaces* **2010**, *2*, 474.
30. Campos, L. M.; Tontcheva, A.; Gunes, S.; Sonmez, G.; Neugebauer, H.; Sariciftci, N. S.; Wudl, F. *Chem. Mater.* **2005**, *17*, 4031.
31. Gurdag, G.; Kurtulus, B. *Ind. Eng. Chem. Res.* **2010**, *49*, 12675.
32. Lee, H. Y.; Bae, D. R.; Park, J. C.; Song, H.; Han, W. S.; Jung, J. H. *Angew. Chem.* **2009**, *121*, 1265.
33. Meng, X.; Wang, Z.; Wang, L.; Pei, M.; Guo, W.; Tang, X. *Electron. Mater. Lett.* **2013**, *9*, 605.
34. Wu, N.; She, X.; Yang, D.; Wu, X.; Su, F.; Chen, Y. *J. Mater. Chem.* **2012**, *22*, 17254.
35. Yang, B.; Guo, Y.; Zhang, S.; Wen, T.; Zhao, C. *RSC Adv.* **2014**, *4*, 64771.
36. Iwan, A.; Boharewicz, B.; Tazbir, I.; Sikora, A.; Zboromirska-Wnukiewicz, B. *Int. J. Photoenergy,* **2015**, DOI: 10.1155/2015/764938.
37. Yang, H.; Fung, S. Y.; Liu, M. *Angew. Chem. Int. Ed.* **2011**, *50*, 9643.
38. Dewitte, H.; Verbeke, R.; Breckpot, K.; De Smedt, S. C.; Lentacker, I. *Nano Today* **2014**, *9*, 743.
39. Roy, S. G.; De, P. *J. Appl. Polym. Sci.* **2014**, *131*, DOI: 10.1002/app.41084.
40. Sharker, S. M.; Kim, S. M.; Lee, J. E.; Jeong, J. H.; In, I.; Lee, K. D.; Lee, H.; Park, S. Y. *Nanoscale* **2015**, *7*, 5468.
41. Kohane, D. S.; Langer, R. *Chem. Sci.* **2010**, *1*, 441.
42. Liu, J.; Wang, X.; Li, D.; Coates, N. E.; Segalman, R. A.; Cahill, D. G. *Macromolecules* **2015**, *48*, 585.
43. Ankareddi, I.; Brazel, C. S. *J. Appl. Polym. Sci.* **2011**, *120*, 1597.
44. Kim, S. H.; Lee, J. E.; Sharker, S. M.; Jeong, J. H.; In, I.; Park, S. Y. *Biomacromolecules* **2015**, *16*, 3519.
45. Qiu, J.; Wang, S. *J. Appl. Polym. Sci.* **2011**, *119*, 3670.
46. Sedó, J.; Saiz-Poseu, J.; Busqué, F.; Ruiz-Molina, D. *Adv. Mater.* **2013**, *25*, 653.